FACULTY OF SCIENCE
UNIVERSITY OF COPENHAGEN

Bachelor Project

Solvej Knudsen and Freja Thilde Pedersen

Producing adiabatic fiber tapers

Numerical simulations and measurements

Supervisor: Assoc. Prof. Jürgen Appel

June 11, 2014

Abstract

High transmittance of tapered fibers is widely desired. In this project we investigate whether this can be reached by shaping the transitions with respect to adiabatic criteria. Through an algorithm, the shaping is simulated, both in one step, and by dividing it into several. Three of these simulated shapes are experimentally performed, and is seen to resembles the simulated. The simulated shapes stays below the adiabatic limit, and our highest transmission at $97.1 \pm 1.7\%$, is reached when pulling in four steps.

Contents

1 Introduction

In modern physics and engineering, optical fibers have numerous applications. Mainly their property to guide and transmit light with very low loss over large distances has made them useful. This low loss feature makes them exceptionally good at transporting information, which is widely desired. Optical fibers are for example used as quantum information carriers, for data transfer and storage, and even for HDTV using their broad bandwidth.
After discovering that optical fibers with very small diameters still guide light with low loss, new possibilities for applications have been discovered. These *nano fibers* have turned out to be useful as beam splitters, as single molecule sensors, and in integrated optics as in-couplers. The property exploited is their ability to have light propagating on the outside of the fiber. When light is guided through the nano section, the mode extends the thin fiber, and light will be guided as an evanescent field. Another interesting application is to use the nano fiber as an atomic trap. The idea is that atoms will couple strongly with the evanescent field around the fiber. To trap the atoms around the fiber, two additional laser beams are applied, one red-detuned and one blue-detuned with respect to the atomic transition. These will respectively attract and repel the atoms, and when the red-detunded beam is a standing wave, they will generate potential minima along the fiber, where the atoms will be trapped. It is this atom trapping application that our project is targeting.
The nano section is very sensitive to environmental disturbances, therefore it is desired to be as short as possible, and usually only a few centimeters are required to trap atoms. The section is reached by gradually decreasing the diameter down to a few hundred nano meters. The shape of this tapering section is very important, as it determines the transmittance through the fiber.
The amount of transmission of the laser beam that couples to the atoms, are essential. If there are losses, we cannot be sure to obtain sufficient information about the atoms. In the transition before the mode extends the fiber, coupling to other modes can happen, which will affect the transmission. Our aim is to produce fibers with transitions designed to avoid the coupling to other modes. From mode guidance theory, such a shape can be calculated. Using this *adiabatic shape* we will simulate how to create this fiber in practise, and afterwards test it experimentally.

2 Theory

In this section, we will describe the optical step-index fiber, and give an outline of the most important theory behind guided modes. This allows us to predict when excitations to higher order modes happen, as the fiber is tapered down. To obtain higher transmittance through the fibers, these excitations must be avoided, leading to a desired target shape of the fibers. In the end, we will present the basic principles in our method to make tapered fibers.

2.1 Single-mode step-index optical fibers

An optical fiber is made of high quality silica (glass) with a diameter on the order of 0.1 mm. In contrast to a graded-index fiber, whose refractive index changes gradually from the center and out, a step-index fiber consists of two layers; a core and a cladding, with slightly different refractive indices as seen in figure 1. The refractive index of the core is slightly larger than the one of the cladding, $n_{\mathrm{co}} > n_{\mathrm{cl}}$, and in the ray optics picture this leads to total internal reflection of light on the interface between the core and the cladding. This means that light can propagate in the fiber core, if the incident angle θ_{i} is such that the internal reflection angle θ is less than the critical angle θ_{c}. The critical angle is the maximum angle for which total internal reflection occurs, and is given as $\theta_c = \sin^{-1}(n_{\mathrm{cl}}/n_{\mathrm{co}})$ [Milonni et al. 2010]. The relative size of the indices of refraction for the core and the cladding is therefore crucial for how easy light can be coupled into the fiber. For a single-mode fiber, the critical angle of the incoming light is so small that only light nearly parallel to the fiber axis is guided. Therefore single-mode fibers are called *weakly guiding*.

The guided modes in a fiber at core radius ρ_{co} are governed by the core guidance parameter, also called the V-parameter:

$$V = \frac{2\pi}{\lambda}\rho_{\mathrm{co}}\sqrt{n_{\mathrm{co}}^2 - n_{\mathrm{cl}}^2}, \tag{1}$$

where λ is the wavelength of the incoupled light. The V-parameter only takes the core and cladding refractive indices into account, meaning it neglect the surrounding air, and assumes an infinite cladding region. The guided fiber-mode in a single-mode fiber is propagating in the core, therefore also referred to as the core-mode. Also higher order cladding-modes exist, which are the possible modes that could be guided in the cladding. When coupling into a fiber, one has to make sure not to couple into a cladding-mode instead of a core-mode. For single-mode fibers the core radius is chosen such that $V < 2.405$, where the higher order modes are no longer guided in the core, but in the cladding instead, and only the fundamental mode is left in the core. This is called the *single-mode cutoff*.

A fiber-mode is defined as a field distribution which, apart from a phase, preserves its form

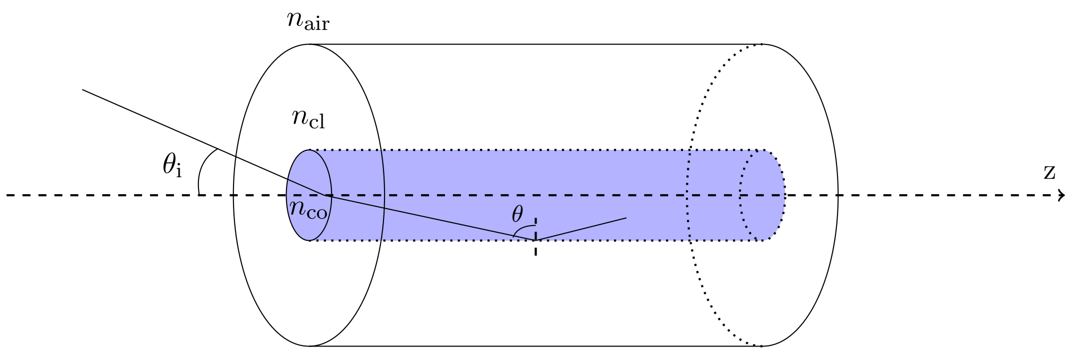

Figure 1: *Step-index optical fiber described in the ray optics picture. The core (blue), has a slightly larger refractive index than the cladding: $n_{co} > n_{cl}$. n_{air} is the refractive index of air and is ~ 1. For light to be guided, it must be incident with an angle such that $\theta \leq \theta_c$.*

while propagating along the fiber axis z. The phase is given by the last exponential in the electric field of the mode, which in cylindrical coordinates is written as:

$$\mathbf{E}(r, \phi, z) \propto \mathcal{E}(r, \phi) \exp(-i\beta z) \tag{2}$$

where $\mathcal{E}$ is the field amplitude, and β is the propagation constant. Assuming an infinitely long and perfectly cylindrical symmetric fiber, β is found by solving the scalar wave equation [Milonni et al. 2010]:

$$\frac{\partial^2 \mathcal{E}}{\partial r^2} + \frac{1}{r}\frac{\partial \mathcal{E}}{\partial r} + \frac{1}{r^2}\frac{\partial^2 \mathcal{E}}{\partial \phi^2} + \frac{\partial^2 \mathcal{E}}{\partial z^2} + \frac{n^2}{\lambda^2}\mathcal{E} = 0, \tag{3}$$

where n is the refractive index in the relevant layer. The infinite cladding assumption is also justified here. For core-guided modes the amount of field in the cladding region are small, and therefore this is a good approximation. After solving equation 3 separately for the two index regions, the full solutions are constructed by requiring the radial intensity distribution to be continuous at the borders, finite at the center and zero at infinity. Solving the eigenvalue equation for the solutions, provides the wanted propagation constant β.
When assuming an infinite cladding region, the fundamental mode is always guided in the core. As we will see, this infinite cladding approximation fails for very small core radii, where the mode volume starts to increase, and extends outside the fiber core. If the finite cladding is taken into account the fundamental mode will at some point effectively start being guided in the cladding instead of the core.

2.2 Light propagation in tapered optical fibers

As long as the weakly guiding approximation holds, the modes propagating in the fiber can be approximated by the LP_{lm}-modes. These modes are **L**inearly **P**olarized, meaning that polarization along the fiber axis is neglected. The intensity profile for the first four LP_{lm}-modes are pictured in figure 2, where the fundamental mode is the LP_{01}.
Coupling between two modes can become effective when the two modes have similar azimuthal spatial symmetry, i.e. have the same l value. Considering figure 2 the fundamental mode would therefore be likely to couple to the LP_{02} mode. Coupling to modes with different symmetry would require breaking the azimuthal symmetry of the fiber. This could happen by heavy bending of the fiber or, e.g. by dust particles causing scattering.

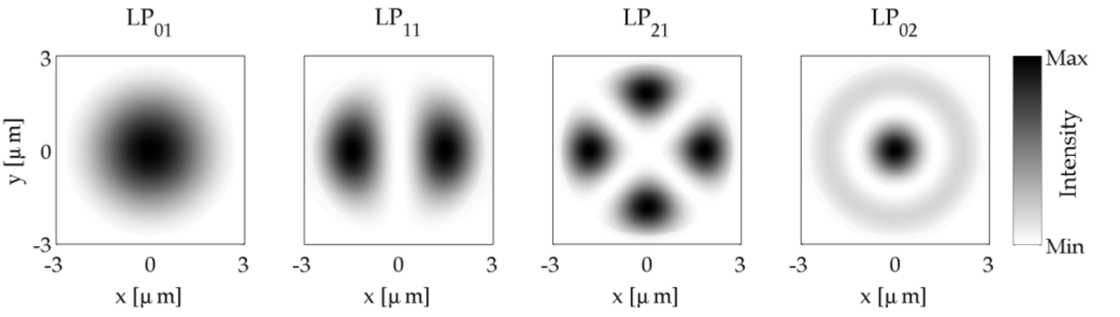

Figure 2: *The transverse intensity profile for the first four LP_{lm}-modes. The picture is taken from [Sørensen 2013].*

2.2.1 Propagation constants for the tapered fiber

The following is a qualitative outline of the most important physical aspects of the derivation of the mode propagation constant and effective refractive indices for a tapered fiber. For a

more thoroughly derivation one should consult [Love et al. 1991].
The electric field of a mode propagating in a tapered fiber is of the form:

$$\mathbf{E}(r, \phi, z) \propto \mathcal{E}(r, \phi) e^{-i \int_0^z \beta(z')\, \mathrm{d}z'}, \tag{4}$$

where the integral of β is the accumulated phase the field experiences during propagation. Opposed to the case with the untapered fiber, β will now change along the fiber axis.
Before the tapered section, the fundamental mode will propagate in the core as described in section 2.1. When entering the tapered region, where the core radius gets smaller, the fundamental mode will propagate more and more in the cladding, affecting the effective index of refraction the field "feels". This is another way of understanding the z-dependent β, since the effective index of refraction is related linearly as

$$\beta = k_0\, n_{\mathrm{eff}}, \tag{5}$$

where $k_0 = 2\pi/\lambda$ is the free space k-vector. The guided modes in the tapered fiber are found, as for the untapered fiber, by solving the scalar wave equation in cylindrical coordinates. It is solved with the appropriate boundary conditions for each point along the z axis as if they where infinitely long cylinders (see the blue lines in figure 3).
When solving the wave equation for the tapered fiber, the infinite cladding approximation is no longer valid, and it must be done in all three regions of different refractive indices. The solutions should connect continuously at the borders just as for the untapered fiber. These continuous solutions leads to the approximate LP-modes. The propagation constants for the modes can be found by solving the eigenvalue equation.

2.2.2 Coupling to higher order modes

The effective refractive indices for each mode can be expressed as a function of the core guidance V-parameter. This can be done, since the ratio of the core and cladding radii is constant, therefore the V-parameter is only proportional to the core radius. The effective refractive indices for the two first LP_{0m}-modes in our fiber are plotted as a function of the V-parameter in figure 4. At large values of the V-parameter we see that both modes are guided in the core. From $V = 2.405$ and down the LP_{02}-mode is guided in the cladding, and this is the before mentioned single-mode cutoff. The value of the V-parameter for our untapered fiber is $V = 2.34$ and is indicated just below the cutoff [Sørensen 2013].
As the core radius decreases, the effective refractive index of the fundamental mode approaches the refractive index of the cladding. In contrast to the infinite cladding solution, the value of the effective refractive index now moves below the cladding value. At some point $n_{\mathrm{eff}_{01}} = n_{\mathrm{cl}}$. This happens at $V = V_{\mathrm{cc}}$ at approximately 0.75, which is called the core-mode cutoff for the fundamental mode. Near V_{cc}, the effective refractive index of the LP_{02} mode is very close to the fundamental mode, and it is when the core tapers down to this point that light can couple into the LP_{02} mode. The curves for the effective refractive indices of the higher order modes are not included in the figure, but will all lie below the LP_{02} cladding mode. Coupling to these modes could in principle also happen, but effectively it will not. Only the second order LP_{02} mode will therefore be considered from now on when trying to minimize coupling to any higher order modes.

2.3 Adiabatic tapering angle

The shape of the tapered section can be described by the angle $\Omega(z)$ at each point along the axis. $\Omega(z)$ is defined as:

$$\Omega(z) = \left| \frac{\partial \rho_{\mathrm{co}}(z)}{\partial z} \right|, \tag{6}$$

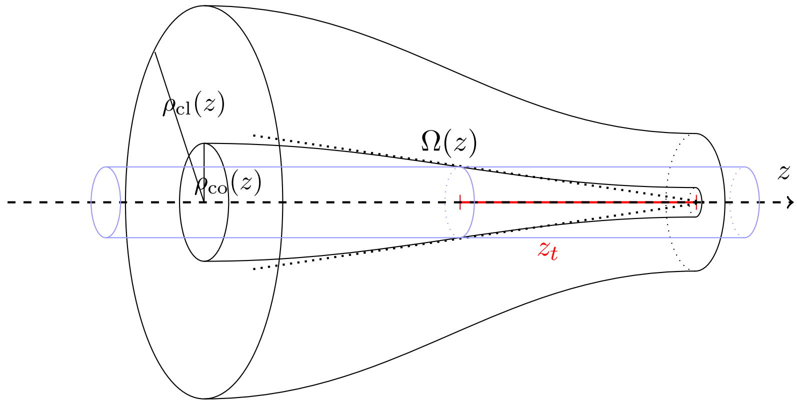

Figure 3: One side of a tapered fiber, where $\Omega(z)$ is the local taper angle. The local taper length is indicated by z_t. $\rho_{co}(z)$ and $\rho_{cl}(z)$ are the core and cladding radii, respectively, along the fiber. The blue cylinder illustrates how all values are calculated as infinite cylinders at each point along the z axis - hence the name local.

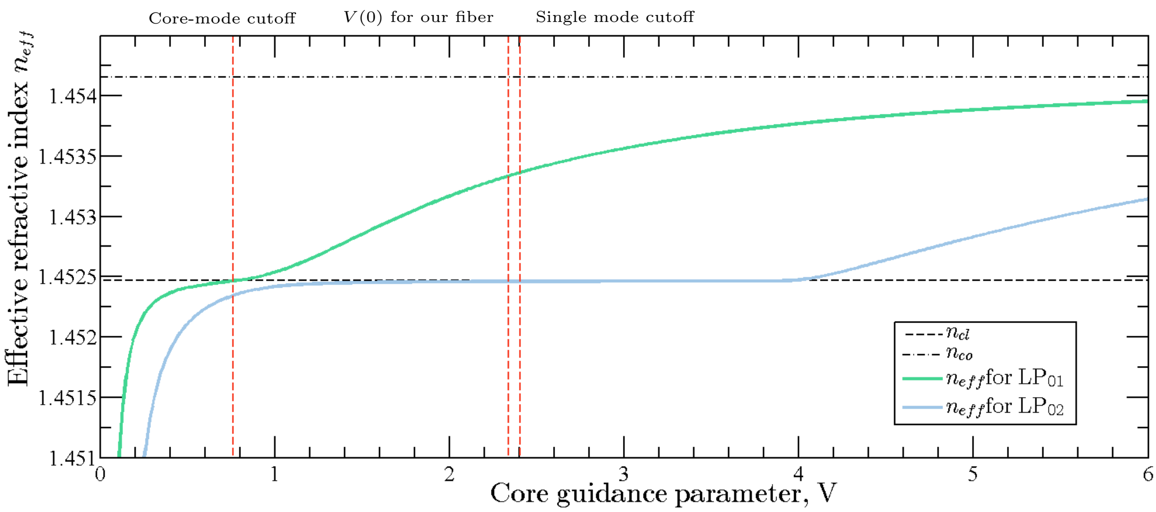

Figure 4: The effective refractive indices of the first two LP_{0m} modes propagating in a step index fiber as a function of the core guidance V-parameter. The calculation is done within the weak guidance approximation and considering finite cladding.

where $\rho_{\text{cl}}(z)$ is the cladding radius and $\rho_{\text{co}}(z)$ is the core radius. These are all pictured in figure 3. It turns out, that by choosing the right tapering angle along the fiber it is possible to minimize coupling to the second order mode. In order to find an upper limiting angle, we will compare the local taper length to the local beat length. The local taper length z_t is shown in figure 3 and is defined through $\Omega(z) = \tan^{-1}(\rho(z)/z_t) \approx \rho(z)/z_t$. In practice $\Omega(z) \ll 1$ and the approximation is justified. When the taper length is long at each point, the tapering angle is slowly varying. The beat length between the fundamental mode and the LP$_{02}$-mode is given by $z_b = 2\pi/(\beta_{01} - \beta_{02})$, where the subscripts refers to the subscripts on the LP$_{lm}$-modes. If the beat length is long, the two propagation constants are similar. This means that the two modes have almost the same phase and are therefore very sensitive to changes along the fiber. We can understand what happens by looking at each of the field modes [Love et al. 1991]:

$$E_{01}(r, \phi, z) \propto \mathcal{E}_{01}(0) \exp\{i \int_0^z \beta_{01}(z')\mathrm{d}z'\}, \tag{7}$$

$$E_{02}(r,\phi,z) \propto \mathcal{E}_{02}(0)\exp\{i\int_0^z \beta_{02}(z')\mathrm{d}z'\}\int_0^z C(z')\exp\{i\int_0^{z'}\beta_{01}(z'')-\beta_{02}(z'')\mathrm{d}z''\}\mathrm{d}z', \quad (8)$$

where $\mathcal{E}_{01}$ and $\mathcal{E}_{02}$ are the field amplitudes. The first exponential in both equations describe the accumulated phase along the fiber for the respective field mode. The maintaining integral in equation 8, contains $C(z)$, which is the coupling coefficient per unit length along the z-axis, and an exponential depending on both propagation constants. This term describes the amount of light from the fundamental mode that effectively will end up in the second mode. The coupling coefficient is illustrated in figure 5, and determines the amount of light, coupling from mode one to mode two. The exponential describes that the light coupling into the second mode along the z-axis, will accumulate different phases compared to each other. The integral in the exponential, arises since the propagation constants change along the fiber axis. The integral containing $C(z)$ will be almost zero, if we integrate over a whole number of beat lengths $z = nz_b$, where n is an integer, and if $C(z)$ is approximately constant within this integration region. In this case the E_{02} field will become nearly zero, and almost no coupling occurs.

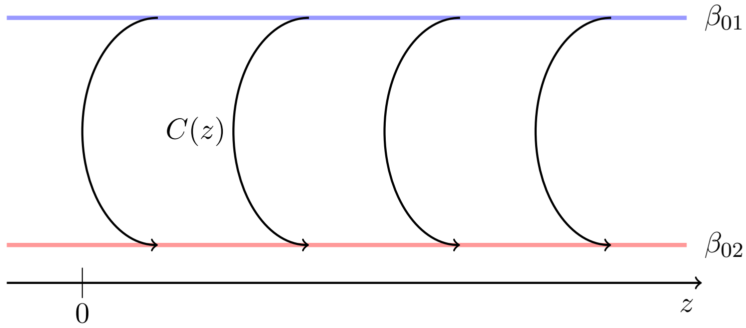

Figure 5: *Arrows illustrate how coupling to the second order mode, happens by light leaking out of the fundamental mode. $C(z)$ is the coupling coefficient per unit time between the two modes.*

The coupling coefficient are proportional to the local tapering angle [Love et al. 1991], meaning that Ω must be slowly varying within a beat length in order to minimize the coupling. Henceforth we require a large taper length compared to the beat length, $z_\mathrm{t} \gg z_\mathrm{b}$. In the other case where $z_\mathrm{t} \ll z_\mathrm{b}$, a significant coupling will happen and light will be lost. Since we are interested in minimal coupling, we can set a limit $z_t = z_b$, which we certainly have to stay below to have an low-loss fiber. Isolating the tapering angle in this equality leads to a boundary on the angles for an approximate adiabatic fiber:

$$\Omega(z) = \frac{\rho_{co}}{2\pi}(\beta_1 - \beta_2) \quad (9)$$

The limiting angle curve $\Omega(z)$ for our fiber is plotted as a function of the normalized core radius in figure 6. The normalized core radius relates to the V-parameter as $\rho_\mathrm{co}(z)/\rho_\mathrm{co}(0) = V(z)/V(0)$, where $V(0) = 2.34$ is the V-parameter for our untapered fiber, and $\rho_\mathrm{co}(0)$ is the untapered core radius. The minimum of the core taper angle is at $\rho_\mathrm{co}(z)/\rho_\mathrm{co}(0) \approx 0.55$, corresponding to $V = 1.28$. This point should be where the refractive indices for the LP_{01} and LP_{02} are closest, and it should approximately correspond to the place where $n_{\mathrm{eff}_{01}} = n_\mathrm{cl}$. This happens at $V = 0.76$, so actually we see a quite large difference between these two values. At values larger than $V = 0.76$ the mode will propagate in the core by the core-cladding interface, and at lower values it will increasingly propagate in the cladding. Here the air will act as cladding for the mode. We had expected the coupling between the two modes to happen when the two refractive indices were closest. It seems like the coupling happens when the fundamental mode is still guided by the core.
Making fibers that stays under this curve will be the task throughout the rest of this project.

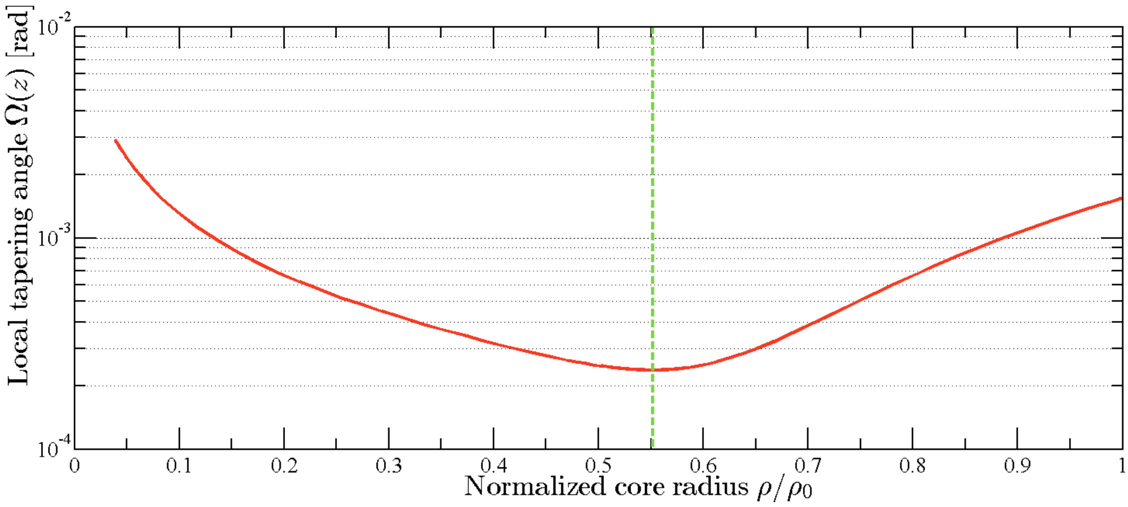

Figure 6: *The limiting angle curve for our fiber, which we want to stay far below to make adiabatic fibers. The green dashed vertical line indicates the minimum of the angle curve.*

2.4 The principle of tapering fibers

Now it's time to consider how we can make tapered fibers. Tapering means to reduce the thickness gradually, and henceforth we will have two tapered sections on each side of the nano section. The idea is to heat up the fiber at one point, so the silica becomes viscous. This heating is done with a small oven. The simplest way to taper a fiber, is to pull each side of the fiber apart, with constant and equal speeds. If the heating is symmetric, the shape will be symmetric around the heated point, when the pulling speeds are constant, and the taper length and final fiber diameter only depends on the total pulling length and the temperature profile of the heater. So a symmetric pull doesn't allow for custom made tapering angles.
To control the local tapering angle, we will use an asymmetric pulling procedure with varying speeds. In this procedure the fiber is fed, with varying velocities, into the oven, and pulled out with constant velocity, on the other side. This asymmetric model is sketched in figure 7. By varying the volume that enters the oven per time, it follows from mass conservation, that we can control the volume pulled out per time. These volumes are indicated with blue in the figure. Since the change in volume per time, can be expressed as the product of the cross-sectional area A and the velocity v, we can mathematically describe the mass conservation as:

$$A_{\text{feed}}(t)v_{\text{feed}}(t) = A_{\text{pull}}(t)v_{\text{pull}} \tag{10}$$

We have assumed that no mass evaporates from the fiber, and that no thermal expansion happens. Furthermore the fiber volume inside the oven is assumed to be heated instantaneous and uniform. This is a good approximation for heaters with a small extension along the fiber axis, and is why the oven is pictured as a plane in the figure.
As mentioned we keep the pulling velocity v_{pull} constant, which makes the pulling length l_{pull} linear in time. In the end we want to express the volume change in equation 10 as a function of l_{pull} instead of time. Rewriting A_{pull} as a function of l_{pull} is straight forward, using $\tilde{f}(l_{\text{pull}}) \equiv f(l_{\text{pull}}/v_{\text{pull}})$, where f is the variable we want to rewrite. A_{feed} on the other hand will be a function of l_{feed}, which again can be expressed as a function of l_{pull}. To relate l_{feed} and l_{pull} it is useful to introduce a new parameter s, defined as the ratio between v_{feed} and v_{pull}. Using that $v_{\text{feed}} = \mathrm{d}l_{\text{feed}}/\mathrm{d}t$ and equivalent for v_{pull}, we can write s as:

$$s = \frac{\mathrm{d}l_{\text{feed}}}{\mathrm{d}l_{\text{pull}}} \tag{11}$$

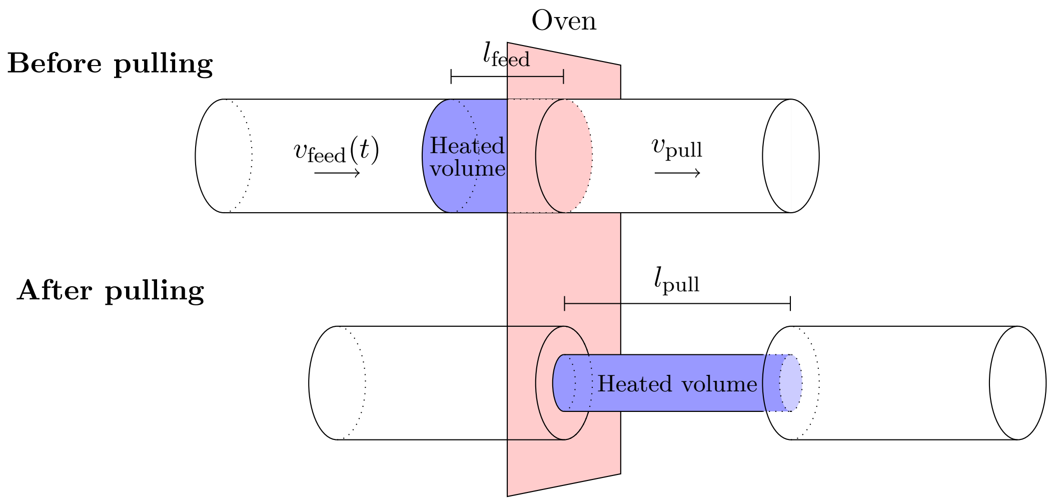

Figure 7: *Pulling model of an asymmetric pull. The oven is pictured as a transverse plane, and the fiber is fed in with varying velocity v_{feed} and pulled out with constant velocity v_{pull}, where $v_{feed} < v_{pull}$. l_{feed} is the length, the fiber is fed into the oven, and l_{pull} is the length pulled out.*

By isolating $\mathrm{d}l_{\text{feed}}$, and integrating over l on both sides we arrive at the following expression:

$$l_{\text{feed}}(l_{\text{pull}}) = \int_0^{l_{\text{pull}}} s(l)\,\mathrm{d}l, \tag{12}$$

We can now write equation 10 as:

$$\tilde{A}_{\text{feed}}(l_{\text{feed}}(l_{\text{pull}}))\tilde{v}_{\text{feed}}(l_{\text{feed}}(l_{\text{pull}})) = \tilde{A}_{\text{pull}}(l_{\text{pull}})\tilde{v}_{\text{pull}}(l_{\text{pull}}). \tag{13}$$

where $l_{\text{feed}}(l_{\text{pull}})$ is given equation 12.
The model presented here is simplified compared to what actually happens when the fiber is pulled through the oven. The oven we use is not simply a transverse plane, instead it has an extension along the fiber axis where it heats with a Gaussian-like profile. Therefore fluid dynamics must be considered in order to describe the flow of the viscous fiber. In the next section, we will see, that this has already been done for our fiber and oven.

3 Prior work

The basis of our project is preceding work, including a pulling setup, and an algorithm or model, which from some specified pulling parameters are capable of predicting the shape of a fiber. In this section we give a short presentation of this setup and the results.

3.1 Prior setup and programs

The experimental setup we use to pull our fibers has been built by Heidi Lundgaard Sørensen, and is described in great details in [Sørensen 2013]. The fiber is pulled by two motorized stages, programmed to move at constant speeds. In the setup, the detection of the transmission through the fiber is possible while pulling. This allow us to see changes in the transmission at each length of elongation of the fiber. After pulling, the fiber can be imaged, and the shape can be determined using an edge-detecting algorithm.

3.2 Simulation and derivation of fluid dynamics in heated fibers

Fluid dynamics has to be considered when describing the behavior of the heated fiber, as mentioned earlier. The continuity equation arising from mass conservation is:

$$-\frac{\partial}{\partial t}A(z,t) = \frac{\partial}{\partial z}\left(A(z,t)v(z,t)\right), \tag{14}$$

where $A(z,t)$ is the cross-sectional area along the fiber, t is time and $v(z,t)$ is the velocity profile of each cross-sectional area $A(z,t)$ along the fiber. If one can solve this equation for $A(z,t)$, the evolution of the fiber shape can be determined. To do this, $v(z,t)$ needs to be known. By turning the problem around, $A(z,t)$ can be measured experimentally, and solving the Navier-Stokes equations, the following expression for $v(z,t)$ is found:

$$v(z,t) = v(z_0,t) + (v_+ - v_-)\cdot\frac{\int_{z_0}^{z}\frac{A_0}{A(z',t)}\tau(z')\,\mathrm{d}z'}{\int_{z_-}^{z_+}\frac{A_0}{A(z',t)}\tau(z')\,\mathrm{d}z'}, \tag{15}$$

where v_+ and v_- are the velocities in each direction, and τ is the fluidity profile. The fluidity profile describes how willingly the fiber mass is to flow and corresponds to the inverse viscosity profile. It can be determined from measurements, and $v(z,t)$ can then be calculated. The profile for our oven turns out to be very close to a Gaussian [Sørensen 2013].

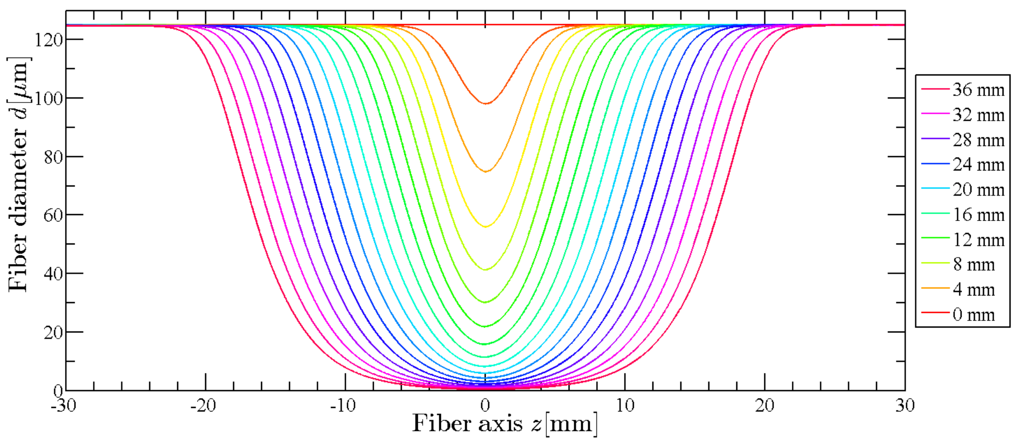

Figure 8: *Simulation of a symmetric pull divided into smaller pulls of two millimeters each, by using the preexisting algorithm. The fiber has been simulated using constant and equal pulling speeds, and the fiber is elongated by* 36 mm. *Legends are only assigned to every second curve.*

Prior to our work an algorithm simulating fiber shapes based on these equations, was written. Using this algorithm we have simulated a symmetric pull, which is elongated by 36 mm and shown in figure 8.

3.3 Transmission and adiabaticity

The transmission for an experimentally symmetrically pulled fiber is plotted with blue in figure 9. The fiber is elongated by 36 mm by using constant speeds of 50 μm/s. The final transmission is $\sim$ 90%, and the loss seems to primary originate from the significant oscillations starting already around elongation length l = 8 mm. An frequency analysis of the signal has been performed using a Gabor transform, which reveals frequencies associated with higher order modes. The frequencies connected to the higher order modes are first seen around an elongation length l = 16 mm.

To relate these excitations with the theory of the limiting angle curve, we have calculated the tapering angle $\Omega(z)$ described in section 2.3, for the simulation of the symmetric pull. We can assume the velocity of the viscous fiber mass in the core and the cladding to be approximately the same while pulling. Henceforth the ratio of the core and cladding radii is constant, and the tapering angle scales linearly. To calculate the angle related to the core radius of the simulated pull is therefore straightforward. The angle curves for each of the 2 mm pulls are plotted together with the limiting angle curve in figure 10. Between normalized core radius $\rho_{\mathrm{co}}(z)/\rho_{\mathrm{co}}(0) = 0.7$ and $\rho_{\mathrm{co}}(z)/\rho_{\mathrm{co}}(0) = 0.4$, the angle curves of the simulated fiber clearly crosses the limiting angle. We believe that the higher order mode excitations seen in the transmission are caused by crossing the limiting angle curve. By instead pulling asymmetrically with varying speeds, we hope to improve the transmission and stay under the limiting tapering angle $\Omega(z)$.

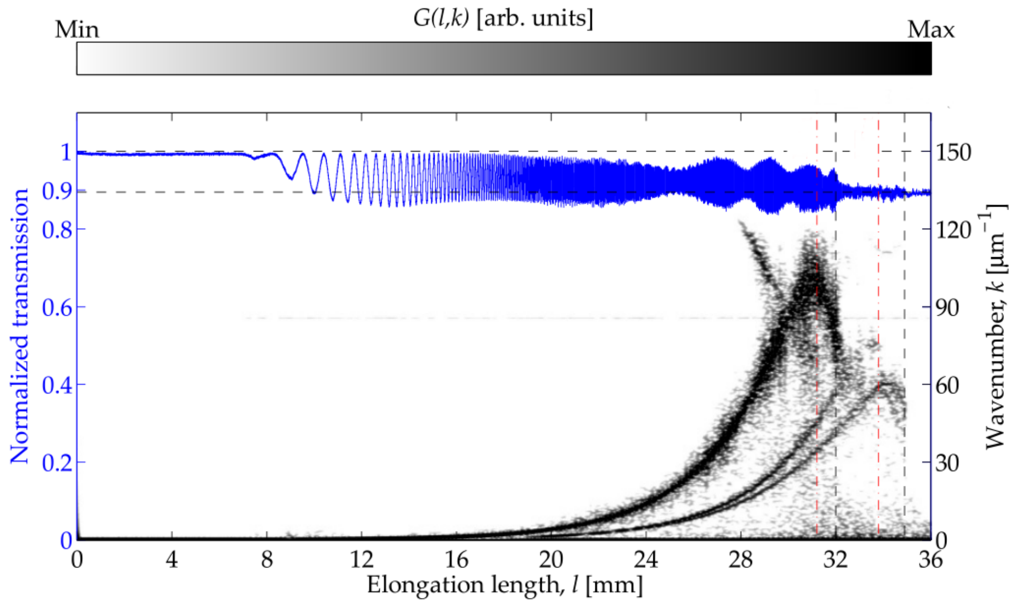

Figure 9: *Transmission curve from [Sørensen 2013] for an experimental pull, with an elongation length of* 36 mm *and constant speeds. We see frequencies related to higher order modes starting at around elongation length* $l = 8$ mm*. The Gabor transform express the present frequencies by their wavenumber. Taken from /citeHeidi.*

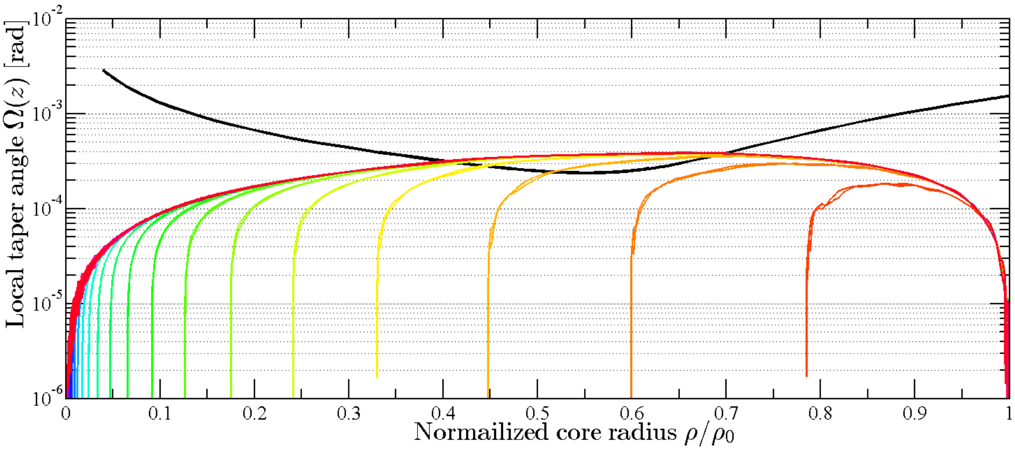

Figure 10: *The black curve are the limiting tapering angle for adiabatic fibers. The tapering angle curves for each of the smaller pulls in the simulated* 36 mm *fiber, are plotted as with the color scheme. The first simulated step, stating from $\rho/\rho_0 = 1$, goes down to ~ 0.9, and then goes back again. This stems from both tapering sides being projected into the normalized radius axis. All the next steps follow, and goes further and further down on the ρ/ρ_0-axis. The angle curves clearly crosses the limiting angle.*

4 The algorithm

We have written an algorithm, which is able to simulate how to pull a desired fiber shape. As it is constructed now, the algorithm probably uses one among many reasonable ways to pull the fiber. We have focused mainly on finding a way to produce adiabatic fibers, using the limiting angle curve discussed in section 2.3, but in principle the algorithm should be able to simulate any shape.

4.1 Outline of the algorithm

A flow diagram of the algorithm is shown in figure 11. To simulate a fiber shape, the following two inputs are required; the shape we want to achieve, referred to as the target shape, and the initial shape of the fiber. Furthermore the simulation can separate the pull into several steps, one have to decide how many. The total number of steps are denoted n, and intermediate steps with i, where $i = 1, 2, ..., n$. A multiple-step fiber are simulated by alternately pulling the fiber through the oven to the right or to the left. We generate an i'th intermediate target shape for each step, and along with the previously simulated shape, we calculate the i'th s-function. This s-function is the same as the s-parameter introduced in section 2.4, given as the ratio of the velocities. The s-function along with the previously simulated shape are used when solving the differential equations, describing the fluid dynamics of the fiber. This provides a fiber shape solution, which now acts as the input parameter for the next iteration. The loop continues until $i = n$.

4.2 Adiabatic target shape

The algorithm simulates the shape of the normalized fiber diameter. In the aim of simulate adiabatic fiber shapes, we have inferred the shape of one transition region from the limiting angle curve, shown in figure 12(a). As expected from the limiting angle curve in figure 6, the slope can be steep in the beginning and the end, whereas it must be moderate in the middle. Here the excitations to the second order mode are most likely to happen. We construct our target shape by mirroring, as we want the same shape for both transition regions. This shape will be the limiting shape, for which theory predicts excitations to happen. To stay

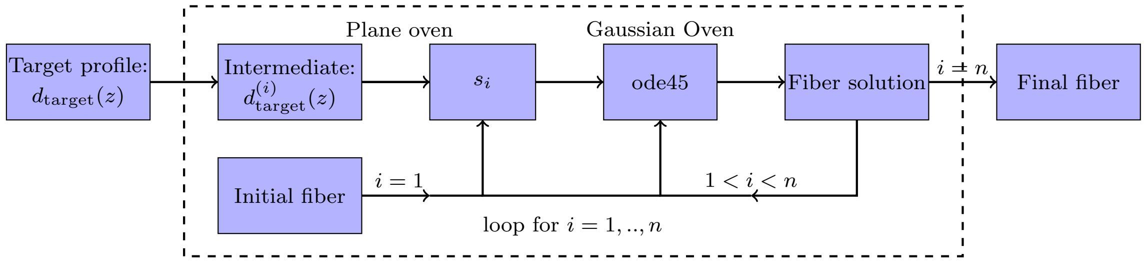

Figure 11: Flow diagram of the algorithm. The algorithm is constructed as a loop, providing an intermediate solution in each step. The final shape is reached when $i = n$.

below this curve, we scale the z-axis by a factor of four. This leads to the target shape in figure 12(b). If the scale are larger, the angle will become accordingly more moderate, and the shape more adiabatic. Upscaling will result in a longer tapered section. Our scaling is chosen to fit the pulling range for our stages.

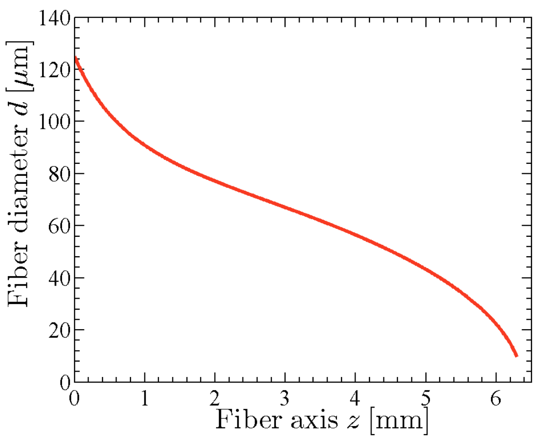

(a) Limiting transition shape. To avoid excitaion of the second order mode, the slope along this trasition should be more moderate.

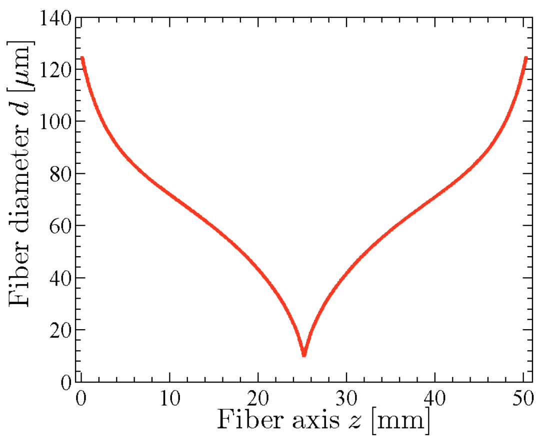

(b) Adibatic target shape generated by mirroring the limiting transition shape. Scaled by a factor of four, to obtain more moderate slopes.

Figure 12: The adiabatic target shape in (b) is obtained by scaling and mirroring the transition in figure (a).

Obviously, we end up with a singularity at the minimum of the target shape. Trying to pull such shape does not seem very physical, and one could choose to implement a flat piece with soft edges to ensure a smooth passage in this point. We haven't done this, since the angle here are allowed to be steep. Furthermore, we want to keep the fiber as short as possible, so it doesn't exceeds the possible pulling range of our stages, while still satisfying the adiabatic criteria. Our target shape only considers the shape of the diameter down to ~ 10 µm, because $\Omega(z)$ cannot be calculated further down within the weakly guiding approximation. In order to use the fiber as an atom trap, the diameter must be ~ 0.5 µm. Even though we don't know the limiting angle at these small diameters, extrapolation of the slope indicates allowance for steep angles. To reach this diameter we suggest to pull a symmetric pull around the minimum of the fiber shape.

4.3 The s-function

As already mentioned the "s"-function (or *the tapering function*) is the ratio of the velocities. It's a smart connection between velocities and the shape of the fiber. Our s-function is inspired by [Baker et al. 2011]. For a one step pull, s is given as:

$$s = \frac{v_{\text{feed}}}{v_{\text{pull}}} = \frac{A_{\text{pull}}}{A_{\text{feed}}}. \tag{16}$$

Here the feeding velocities and areas, are interpreted as parameters for the unpulled fiber, therefore:

$$s(z) = \frac{A(z)}{A_0} = \frac{d^2(z)}{d_0^2}, \tag{17}$$

where $d(z)$ is the target diameter along the fiber, and d_0 is the diameter of the unpulled fiber. Stating s this way assumes a box shaped fluidity profile of the oven used. Even though this differs from our oven, we will calculate s this way, and only when solving the differential equation the Gaussian oven is taken into account. As in [Baker et al. 2011], we want to divide our pulls into several consecutive steps, so each pull can correct for the imperfections caused by the previous one and the deviation from the target shape, can be reduced.

4.3.1 Multiple-step approach

When pulling in multiple steps, our approach is to take the (i/n)'th root of the target shape. This way the target diameter will be reached through multiple steps. The length of the tapered section has to be modified additionally, to avoid the final diameter profile to be much broader than the profile for the target shape. We do this by scaling the axis of each intermediate target profile by i/n. Calculating the intermediate target profiles this way is a choice, which ensure that we distribute the pulling over all intermediate pulls. Putting this into formulas the intermediate shapes are:

$$d_{\text{target}}^{(i)}(z) = \left(d_{\text{target}}\left(\frac{z}{i/n}\right)\right)^{i/n} \tag{18}$$

To calculate the s_i-functions for the multiple steps, we divide these intermediate target shapes with the previously simulated fiber shape. The previous solution corresponds to the feeding cross-sectional area, discussed in section 2.4. It therefore depends on l_{feed}, which is dependent of l_{pull}. The squared target profile corresponds to the pulling cross-sectional area. Thus the intermediate s-functions are:

$$s_i(l_{\text{pull}}) = \frac{A_{\text{target}}^{(i)}(l_{\text{pull}})}{A_{\text{sol}}^{(i-1)}\left(\int_0^{l_{\text{pull}}} s(l)\,\mathrm{d}l\right)}, \tag{19}$$

The profiles of the s-functions used in a 2-step pull are shown along with the intermediate target profiles in figure 13.

When calucalating the s-functions in this way, the $s_i(l_{\text{pull}})$ will try to correct for the errors made, when simulating the previous solutions. If the previous iteration has simulated the diameter profile too broad, the next s-function will suggest to compress the fiber. Since we are not interested in compressing the fiber, the algorithm shifts the position of the target function along the fiber axis, relative to our intermediate target profile. Looping over different shifting values, the s-function that suggests to compress the fiber the least, is chosen.

4.4 The differential equations

The differential equation we solve to simulate the fiber pulling, is based on the preexisting differential equations 14 and 15. We simulate asymmetric pulls in both directions, so we have split the differential equations into two. We can express these differential equations in terms of s. By changing the ratio of the velocities we can control the output shape of the

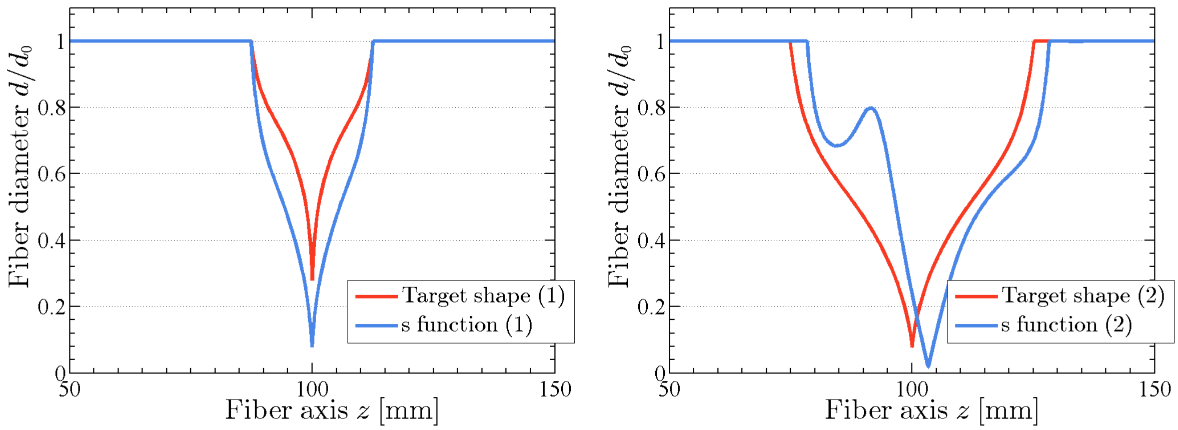

(a) The s_1-function along with the $d^{(1)}_{\text{target}}(z)$ shape for a 2-step pull.

(b) The s_2-function along with the $d^{(2)}_{\text{target}}(z)$ shape for a 2-step pull.

Figure 13: *The two intermediate profiles for s and d_{target} in a 2-step pull.*

fiber. We can rewrite the two equations in the same way as was done in section 2.4, and the resulting differential equation for pulling to the right, becomes:

$$-\frac{\partial}{\partial l_{\text{pull}}}\tilde{A}(z,l_{\text{pull}}) = \frac{\partial}{\partial z}\left(\tilde{A}(z,l_{\text{pull}})\tilde{v}(z,l_{\text{pull}})\right), \tag{20}$$

where

$$\tilde{v}(z,l_{\text{pull}}) = 1 + (1 - s(l_{\text{pull}}))\frac{\int_{\infty}^{z}\frac{\tau(\zeta)}{\tilde{A}(\zeta,l_{\text{pull}})}d\zeta}{\int_{-\infty}^{\infty}\frac{\tau(\zeta)}{\tilde{A}(\zeta,l_{\text{pull}})}d\zeta}. \tag{21}$$

When solving equation 20 for $\tilde{A}(z,l_{\text{pull}})$, we obtain the shape of the pulled fiber. For a multiple-step pull, the solution will be input for the next iteration of the loop, until iteration n. In MATLAB, the differential equation is solved using the ode45-function.

4.5 Simulation results

The algorithm produces simulated fiber shapes, and in the following we will see how well they resemble the target shapes. To see whether the discrepancy from the target shape is reduced, when performing multiple-step pulls, the deviation is calculated for a 1-step up to a 20-step pull. The deviation is shown in figure 14, and calculated by integrating the absolute difference between the normalized simulation and normalized target shape: $\int |d_{\text{target}} - d_{\text{sol}}|\,\mathrm{d}z$. If the two are perfectly consistent this value should be zero.

We see a clear improvement between pulling in one step and four steps. From the 4-step pull to around the 10-step pull the deviation almost doesn't change, and after ten steps the deviation seems to slowly grow again. The 4-step pull provides one of the smallest deviations, and is still within the experimental manageable range. Therefore we have chosen a 4-step pull to be the one we test experimentally along with a 1-step pull. For now we will look into how well these resemble the target shape, and whether stay below the limiting angle curve.

A 1-step and a 4-step fiber shape is plotted along with the target shape in figure 15. Both simulated shapes resembles the target shape well. The deviations are respectively 4.25 and 1.95, and this improvement is also clear when comparing figure 15(a) and figure 15(b).

The 1-step is asymmetric, with its minimum displaced to the left compared to the target minimum. This asymmetry is caused by the asymmetric pulling procedure. If instead the pull was simulated to the left, the asymmetry would be at the other side. In the middle

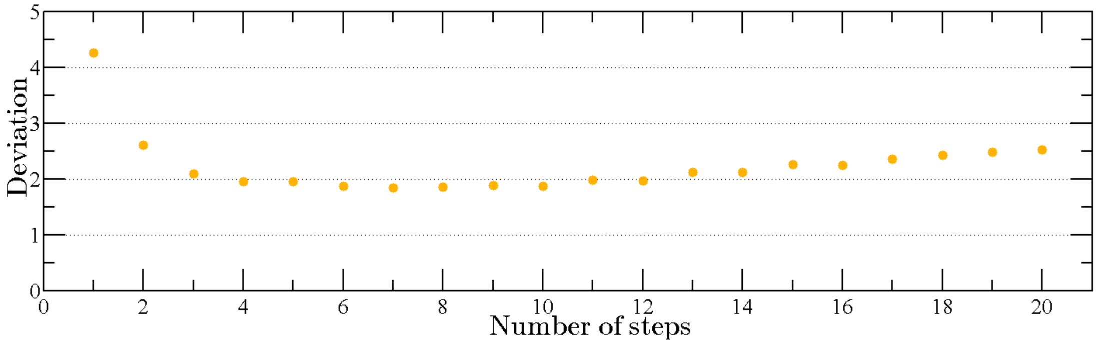

Figure 14: *Deviation of the simulated shapes with respect to the target shape, as a function of the number of steps.*

of the left transition, the slope is much steeper than the slope of the target shape. In the end this could be vital for the adiabaticity of the fiber, since this is exactly in the critical area. For the 4-step, the asymmetry has been smoothed out, and might therefore be more adiabatic. In both cases the final simulated shape is a bit wider than the target shape. This extra width stems from our oven having an extension along the fiber axis, and since our method to calculate s, does not take this into account, additional modification must be done to avoid this.

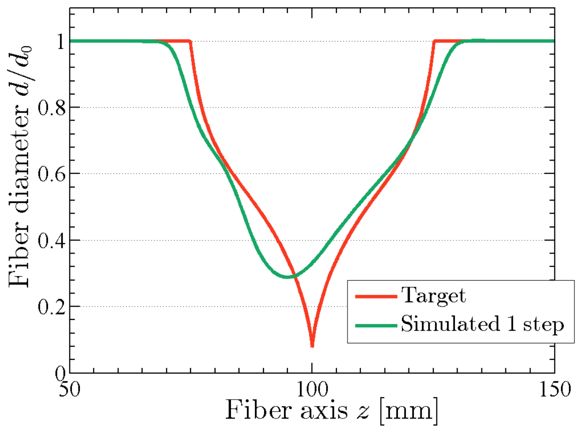

(a) 1-step pull compared to the target shape.

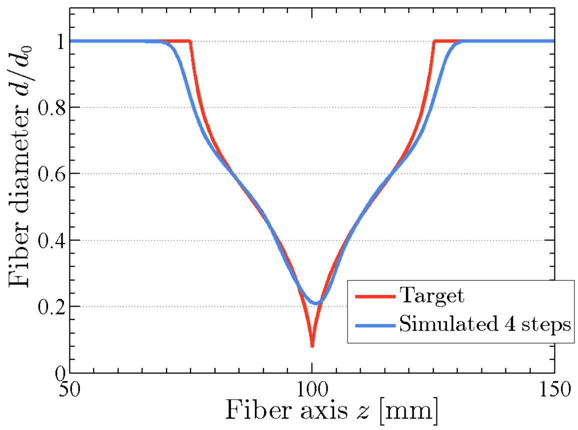

(b) 4-step pull compared to the target shape.

Figure 15: *Simulated fiber shapes compared with the target shape. The 4-step pull is chosen to be compared to the 1-step pull, as there is a significant reduction in deviation compared to the target shape.*

It is interesting that the deviation at some point becomes slightly larger again. When comparing the shape of a 20-step pull to the target shape, the simulation becomes a little too wide. An explanation could be that it is difficult for the algorithm to divide the pull into this many steps. A plot of the 20-step pull can be found in the appendix.

4.5.1 Comparing to the limiting tapering angle

As in section 3, we will compare the simulated shapes to the limiting tapering angle. This is plotted in figure 16. We see that both curves stay below the limiting angle curve. The steep angle in left side of the 1-step pull distinguishes itself by being closer to the limiting curve. Looking at the intermediate solutions for the 4-step pull, reveals that also this fiber was at some point close to the limiting curve, as seen in figure 17.

Even though both simulations come close to the limiting curve, they seem to stay below. When testing these pulls experimentally, it will become evident whether the angle curves stay far enough below the limiting curve. If this is the case, we should avoid excitations of the higher order modes and get a reasonable transmission.

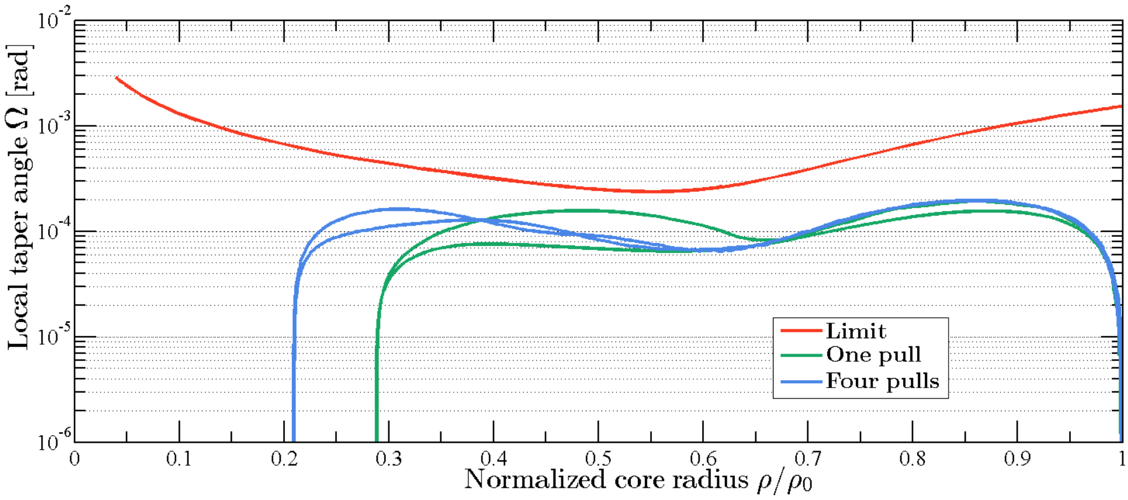

Figure 16: *The angle curves corresponding to a 1-step and a 4-step pull.*

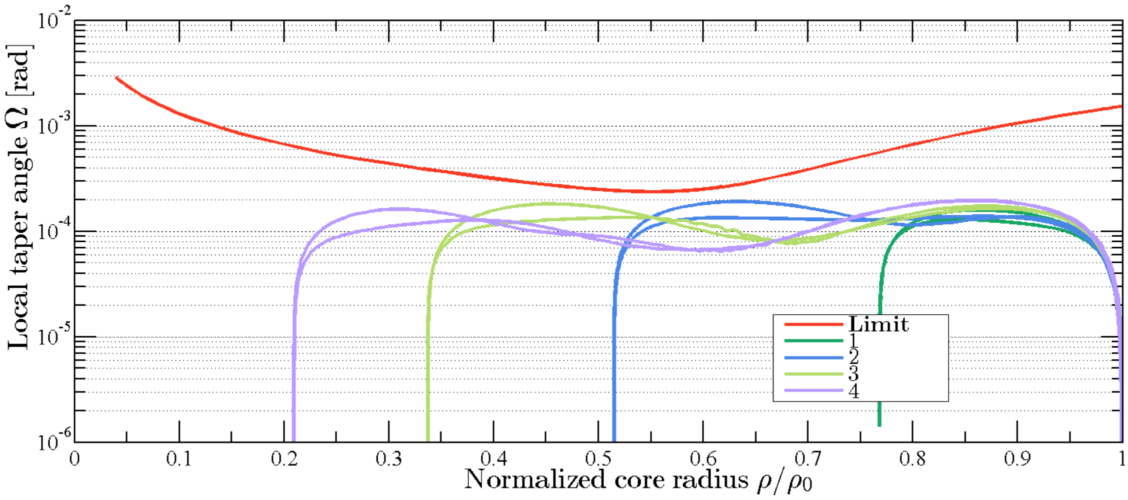

Figure 17: *Intermediate angle curves for a 4-step pull. This reveal that none of the intermediate pulls, intersects with the limiting curve, even though two of them come close.*

5 The experiment

Aiming for a higher transmission through the fibers, we have looked through modal theory of fibers and thereby calculated a limit, by which we can avoid coupling into other modes. This has led to a desired target shape of the fiber. Through an algorithm using differential equations describing the fluid dynamics of the flow in a heated fiber, we have obtained a simulation resembling the target shape. We now want to test whether we can produce this simulated shape experimentally, and in the end obtain the higher transmission. First we will outline the setup, and afterwards we will present our achievements.

5.1 Experimental setup

The setup is schematically pictured in figure 18. The fiber is 125 ± 2 µm in diameter with a 5.5 ± 0.5 µm core. A 852 nm laser is permanently coupled into one end of the fiber, while the other end can be coupled into a photo detector, in order to measure the transmission. After stripping off a protective plastic coat and cleaning that part of the fiber, it is placed in two clamps, approximately 10 cm apart. On the outer side of these, magnetic clamps are holding the unstripped fiber in two V-shaped grooves. The clamps holding the fiber, are sitting on top of two mounts, each of which are standing on a motorized stage. These stages are placed on top of each other, which means that the bottom stage translates the fiber, while the top stage does the actual pulling.
An oven (electric ceramic micro heater) is connected to the system with a motorized rail, and can be driven in between the clamps, to heat the fiber. The mounts and the oven are aligned with respect to each other, so the pulling is approximately in one dimension. After the pulling, the oven is driven out and a CCD camera can be placed instead, to image the fiber shape. The entire setup is placed in a flow box, in order to minimize dust particles. For a more detailed description of the setup see [Sørensen 2013].

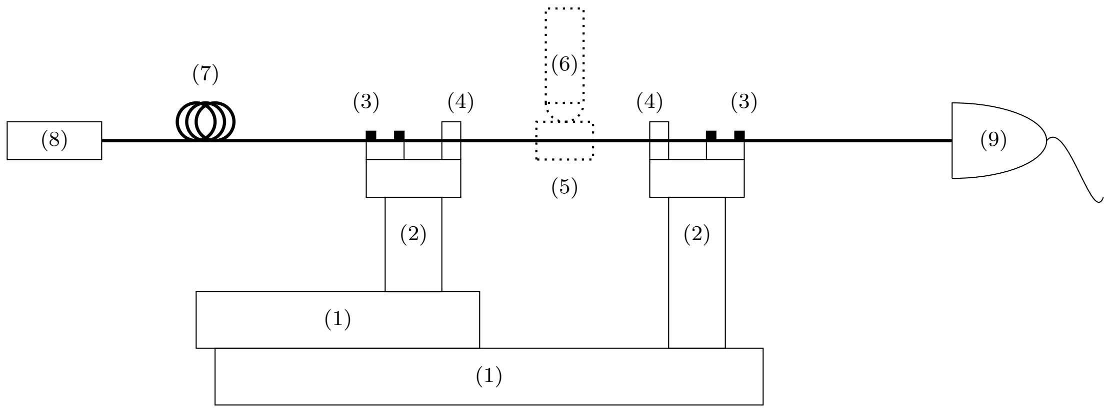

Figure 18: *Schematic drawing of the setup. The stages (1) are stacked i.e. the bottom stage translates the fiber (7), while the top stage does the actual pulling. On the mounts (2) are magnetic clamps on V-grooves (3) along with the new clamps (4), which hold the fiber. The laser (8) is coupled into the fiber in one end, and a photo detector (9) is coupled to the other end. The oven (5) and the camera (6) are indicated with dotted lines, as only one of them can be in the setup at a time.*

5.1.1 Our contribution to the experimental setup

While working with this project, there are mainly four points, where we have changed the setup compared to the one existing.

1. **New clamps:** The V-shaped grooves holding the fiber with strong magnetic clamps, are from the original setup. In these grooves the unstripped fiber is placed. The positioning of the fiber is therefore sensitive to variations in the size of the protecting coat, and could give rise to transverse tension. To improve the accuracy of holding the fiber, we have applied two new clamps holding on the stripped part.

2. **Oven temperature:** After experiencing the fiber slipping under the clamps and magnets, we found that the previously used power (100 W) applied to the oven, didn't provide the necessary temperature to heat the fiber anymore. We haven't identified the reason for this, but it could be that the oven is getting old. After a simple test with a light weight in the end of a heated fiber, we have raised the power to $P = 113$ W.

3. **Reference detector:** We have applied a reference detector, by splitting the laser beam, before it is coupled into the fiber. This allows us to see any instabilities in the laser.

4. **Stages program:** The program that controls the stages has been rewritten[1], so it can follow a given trajectory, requiring varying velocities during one pul, which are provided by our algorithm as data tables.

5.1.2 Performing the experiment

Cleaning procedure
According to [Hoffman et al. 2014] the cleaning procedure is very important, for the resulting transmission. If a dust particle gets heated with the fiber, it can melt into the glass, and cause the laser light to scatter away, or even break the fiber.
After stripping the fiber, the remaining plastic and other impurities are wiped away, and it is checked for dust using the camera. Only when no dust particles are left on the fiber, it is declared ready for pulling.
We have cleaned using tissues and technical grade ethanol as in [Sørensen 2013], and occasionally this provided troubles. At some point we switched to technical grade acetone instead, with similar results. We tried to improve our cleaning procedure by wiping with acetone and tissues followed by spectroscopic grade ethanol and lens paper. This procedure didn't enhance the results, it actually seemed like it provided a lot more dust particles to the fiber. With this observation we have returned to using acetone and tissues, and just wipe several times until the fiber is clean. A last improvement was done using hairnet when cleaning, this seemed like it had a significant effect, but as we have only tried this a few times, it's hard to draw a final conclusion on this. **Tension and alignment**
When placing the fiber in the clamps, we make sure to stretch the fiber, so it does not bend. We ensure proper stretching by moving the top stage ~ 0.09 mm back, while watching if the fiber moves on the camera. If it does not move, it is stretched. We have experienced, that when we drive the oven in and out, without pulling, the fiber gets deformed. This can be seen on the fiber in figure 20, just before the tapering section to the left. An explanation could be that the fiber is over tensed, and as it is heated it is relaxed. Therefore we release the tension by one fifth of the stretching length. Since we still see the effect, other explanations can be misalignment, which we also have tried to improve, or that the fiber is bending from sitting on a spool. As long as the deformation doesn't affect the transmission, this should not be a problem.
After we have pulled a fiber, it is usually bending a bit. Before imaging the fiber, it is therefore stretched, to make it stay in focus along the whole fiber length. **Pulling in multiple steps**
When we pull in multiple steps, we pull several individual pulls consecutively i.e. we upload a new pulling trajectory to the stages between each pull. This happens while the oven is still in. The trajectory is written such that the stages accelerate before entering the actual trajectory producing the tapering section. Furthermore, the algorithm has introduced a shift between each step, so this has to be taken into account too. This whole procedure, could probably be optimized quite a lot, so the whole procedure happens in one take.

5.2 Experimental results

Based on the deviation plot in figure 14, we decided to experimentally pull a 1-step fiber and a 4-step fiber. Since the laser used to measure the transmission made a mode-jump during the tapering of the 1-step pull, we decided to make another 1-step pull with the laser

[1] by Jürgen Appel.

properly stabilized. The two 1-step fibers make it possible to test if the shape of the fiber is reproducible. A picture of the 4-step fiber and the first 1-step fiber are shown in figures 19 and 20. The pictures are composed[2] of many individual CCD camera frames stitched together. A picture of the second 1-step fiber can be seen in the appendix.

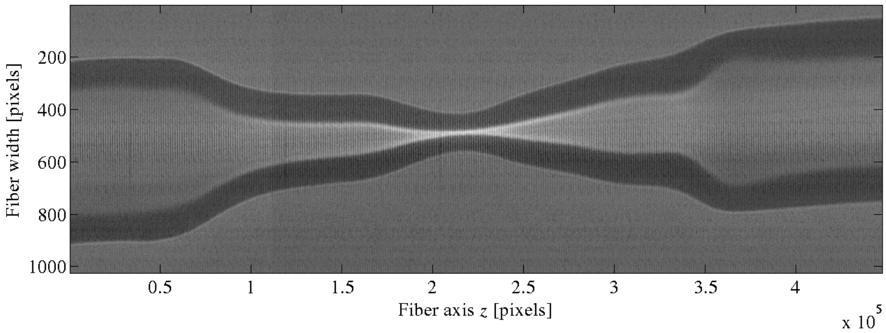

Figure 19: *A picture of the 4-step fiber. Note the extreme difference in scale on the transverse and longitudinal axis.*

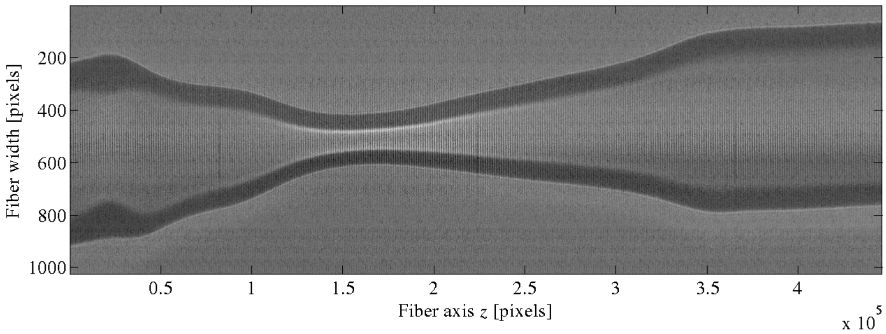

Figure 20: *A picture of the first 1-step fiber. Note the extreme difference in scale on the transverse and longitudinal axis.*

5.2.1 The fiber shapes compared to the simulations

To see whether our tapered fibers are adiabatic, we want to compare them to their respective simulated fiber shapes. In figure 21 the second 1-step fiber and the 4-step fiber are plotted with their simulated fiber shapes. In both cases, the experimental shapes resemble the simulated. We see that especially our 1-step pull matches well, though the depth differs by 5.6 %. The experimental 4-step pull unfortunately deviates from the simulated shape in precisely the critical region. In each single step errors can enter. Therefore the deviation in the 4-step pull can be due to accumulation of such errors. This deviation can possibly be reduced by optimizing the multiple-step procedure. The 4-step pull is also not perfect, but a little better, as the deviation is 5.2 %.

5.2.2 Reproducibility of the fibers

To see whether we are capable of reproducing the shapes, the two 1-step pulls are compared in figure 22. The two shapes are very similar except for the small deviation at the beginning of the tapered section. This could be due to the problems we have had with the small deformation in the left side of the fiber. The deformation of the fiber can also be seen in figure 20 in the far left side. The deviation in the depth between the two pulls are only 1.0

[2]The pictures are generated by an imaging algorithm described in [Sørensen 2013].

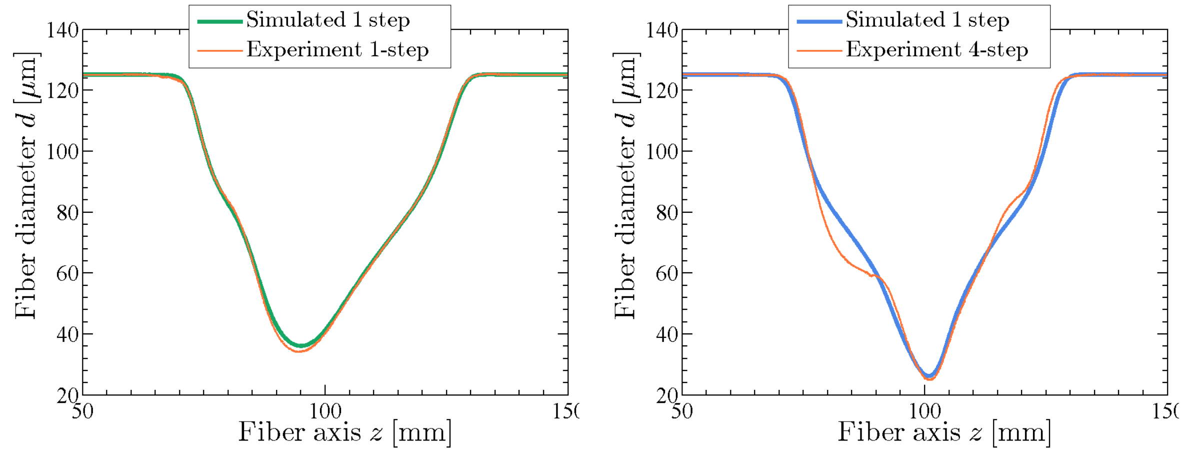

(a) The experimentally tapered 1-step fiber compared with the simulated 1-step fiber.

(b) The experimentally tapered 4-step fiber compared with the simulated 4-step fiber.

Figure 21: *The shapes of the experimentally pulled fibers follow the shape of the simulated fiber well.*

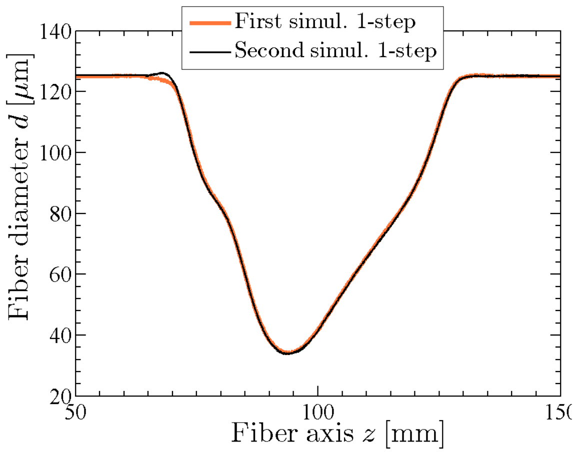

Figure 22: *The two experimentally pulled 1-step fibers compared, in order to check reproducibility.*

%, meaning that it seems like the experimental shapes are reproducible.

5.2.3 Transmission

The essential quality of our adiabatic shaped fibers are their transmittance. The transmission detected during the three experimental pulls is presented in figures23, 24 and 25. The percentage transmissions are $93.2 \pm 1.4\%$, $96.5 \pm 1.5\%$ and $97.0 \pm 1.7\%$ respectively. These are calculated from the mean values at each end, delineated by the red lines in the figures. The errors are obtained through error propagation using the standard deviations in the same delineations. The transmission is normalized with respect to the mean value in the left delineation. We see that the signals don't get to stabilize in the end, as we never pull all the way down to the nano section. This means that our transmission results are not to be taken as final values, but is seems like we have past the critical part of the tapering with a high transmission.
Using our pulling method we seem to achieve relatively high transmissions. Comparing to the transmission for the symmetrical pull in figure 9, all the fast oscillations are avoided, and it seem like we almost don't couple to higher order modes. Although, in both of the 1-step transmissions we see some slow oscillations. We cannot immediately address these as higher order modes, and their origin is still to be found.

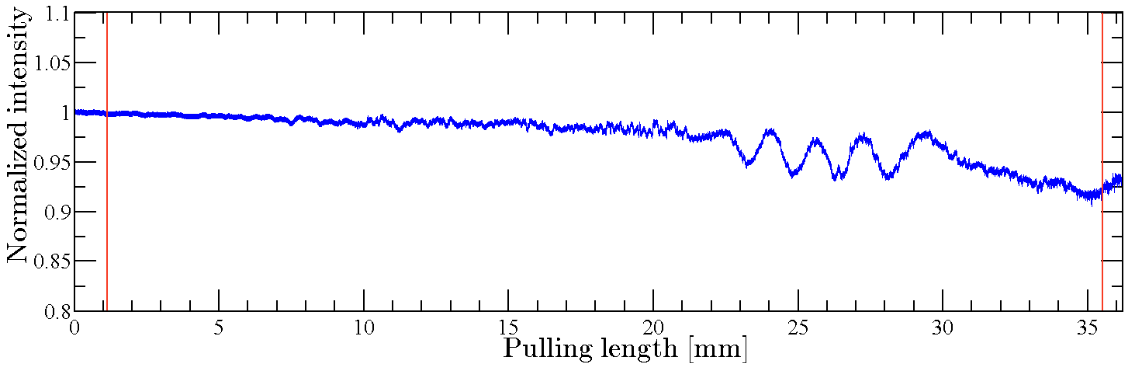

Figure 23: *Normalized transmission for the first 1-step fiber. The red vertical lines indicate the 60,000 points in each end used to calculate the transmission.*

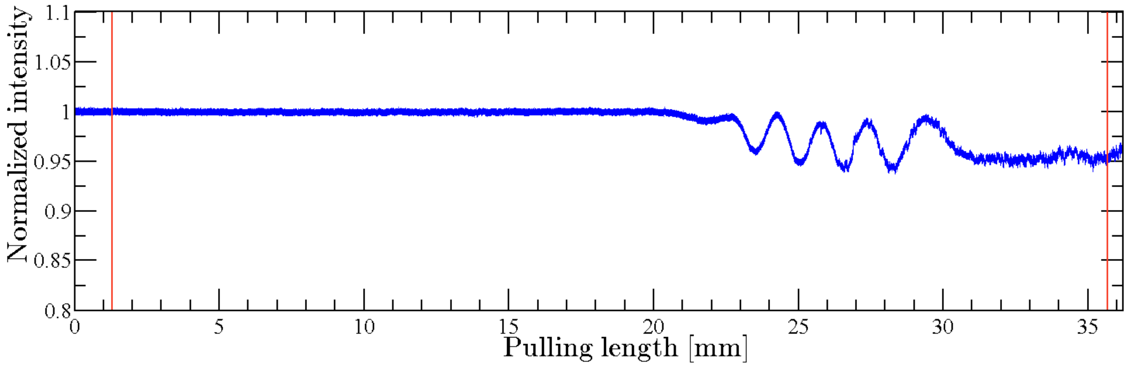

Figure 24: *Normalized transmission for the second 1-step fiber. The red vertical lines indicate the 60,000 points in each end used to calculate the transmission.*

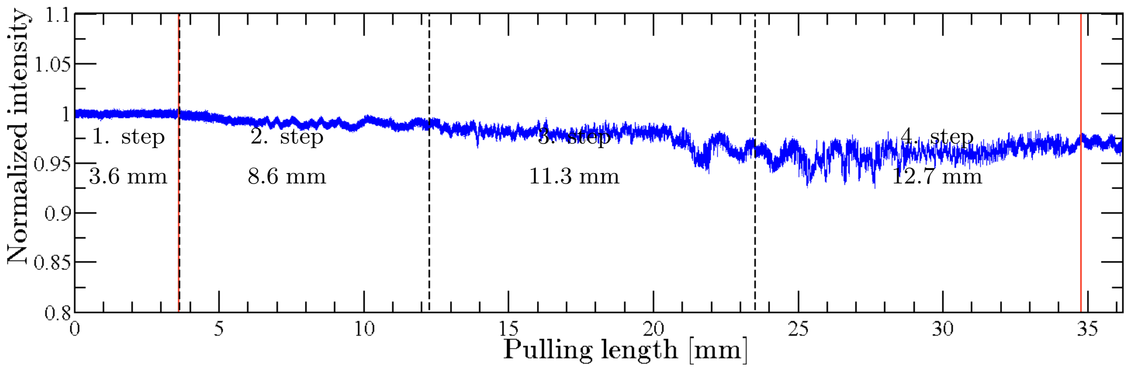

Figure 25: *Normalized transmission of 4-step fiber. The transmission during each step has been recorded independently, and manually appended. The red vertical lines indicate the 130,000 points in each end used to calculate the transmission.*

For the 4-step the transmission are recorded individually in each step. These steps are appended and indicated with vertical dashed lines in figure 25. In addition to the slow oscillations, the transmission of the first 1-step pull in figure 23 are constantly decreasing. The reference signal is shown in figure 26, and as this signal do not decrease, this is probably due an unstable incoupling to the fiber. The reference signal clearly jumps at some point, which indicates a mode jump in the laser. Thus having a reference detector is necessary, as the laser can be unstable. In this case the transmission is not reliable. After pulling the first 1-step fiber, we hoped to address the oscillations to this instability in the laser, but almost identical oscillations showed up in the second pull.

Our theory only considers excitation to modes with the same azimuthal symmetry. Coupling to modes with other azimuthal symmetry could happen, if the fiber becomes slightly asymmetric during the pulling. The observed slow oscillations in the transmission could stem from this.

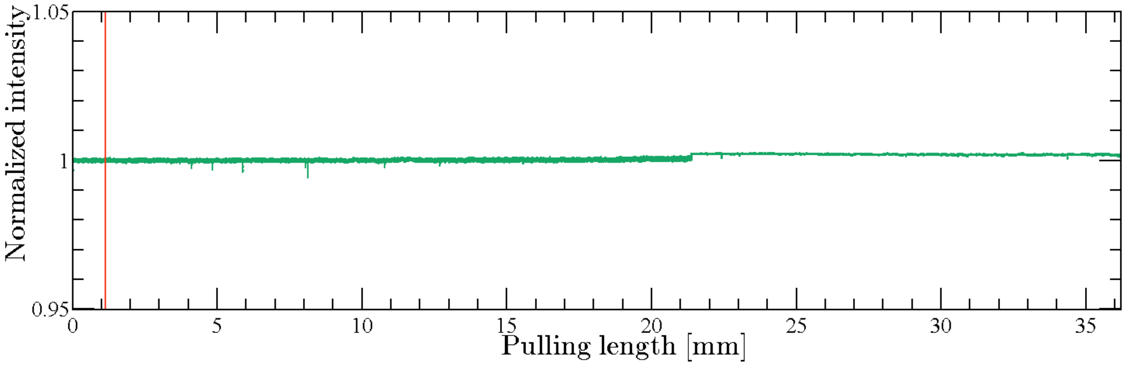

Figure 26: *Normalized reference signal transmission for the first 1-step fiber. Note the different scale in the vertical axis, compared to the signal in the previous transmission figures.*

6 Conclusion and outlook

We have improved the transmittance of our tapered fibers though shaping them adiabatically. Our best achievement are $97.1 \pm 1.7\%$. Using our algorithm, we are able to simulate the changing ratio of velocities, needed to pull the adiabatic target shape. The shaping is performed well by the asymmetric feeding and pulling procedure.
Based on our considerations, this approach could with time become a significant contribution, in the production of fibers for atomic traps. When comparing the adiabatic target shape to the simulation, and the simulation to the experimentally produced shape, they resemble well. This implies that the structure of the algorithm are pointing in the right direction, but are still to be optimized. For example the calculation of the intermediate target shapes, could be interesting to explore.
The algorithm is constructed to take any target shape as input. Therefore it might be possible to incorporate our algorithm in the production of nano fibers for other applications.
The slow oscillations observed in the transmission, implies that we still couple to higher order modes. Apart from break in the azimuthal symmetry of the fiber, the oscillations could somehow be connected to the discrepancy seen in section 2.2.2, between the minimum of the limiting angle curve and the core-mode cutoff for the fundamental mode. This discrepancy should be thoroughly investigated.

A great thanks to: Heidi Lundgaard Sørensen, Jörg Helge Müller, Stefan Christensen and JB for their valuable time and support.

References

[Milonni et al. 2010] P. W. Milonni & J. H. Eberly (2010). *Laser Physics*, sec. 8.6-7. John Whiley & Sons, Inc. ISBN 978-0-470-38771-9.

[Love et al. 1991] J. D. Love, W. M. Henry, W. J. Stewart, R. J. Black, S. Lacroix, F. Gronthier (1991). *Tapered single-mode fibres and devices.* IEE Proceedings-J, Optoelextronics 138.5, pp. 343-347, with appendix 10.

[Baker et al. 2011] C. Baker & M. Rochette (2011). *A generalized heat-brush approch for precise control of the waist profile in fiber tapers.* Optical Materials Express Vol. 1, No. 6, p 1065-1076.

[Sørensen 2013] H. L. Sørensen (2013). *Controlling the shape of subwavelength-diameter tapered optical fibers.* Niels Bohr Institute, Faculty of Science, University of Copenhagen.

[Hoffman et al. 2014] J. E. Hoffman, S. Ravets, J. A. Grover, P. Solano, P. R. Kordell, J. D. Wong-Campos, L. A. Orozco, S. L. Rolston (2014). *Ultrahigh Transmission Optical Nanofibers.* arXiv:1405.3258v1.

[Sørensen et al. 2014] H. L. Sørensen, E. S. Polzik, J. Appel (2014). *Heater self-calibration technique for shape prediction of fiber tapers.* Journal of lightwave technology. arXiv:1312.3840.

Appendix: Fibers

Appendix figures included in the same order as they are mentioned in the main text:

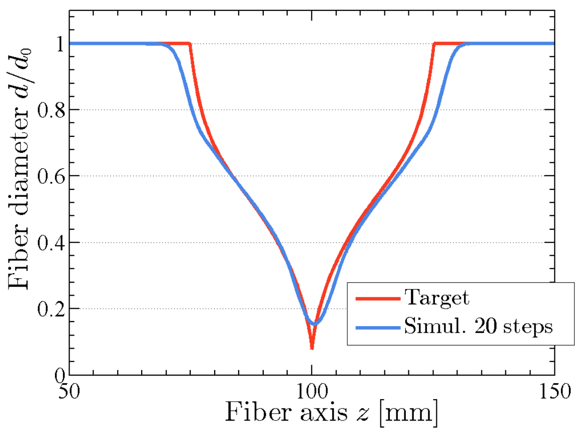

Figure 27: *20-step pull along with the target shape*

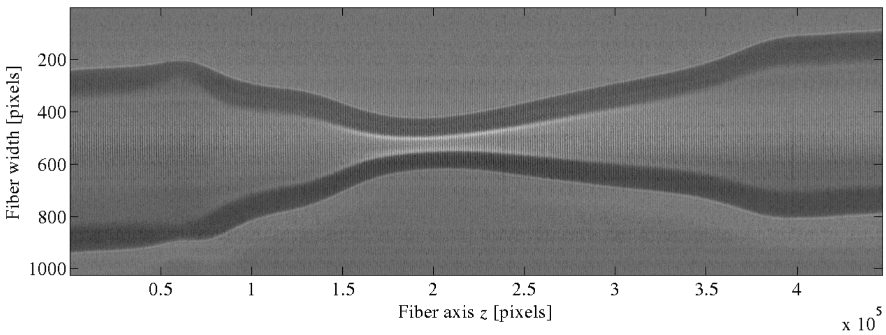

Figure 28: *A picture of the second 1-step fiber, made out of several pictures, taken with the CCD camera, and merged together. Note the extreme difference in scale between the horizontal and the vertical axis.*